Fall 2016

Surface modification of tin oxide nanoparticles by atomic layer deposition for enhanced electrochemical performance

Sai Abhishek Palaparty

Department:

SURFACE MODIFICATION OF TIN OXIDE NANOPARTICLES BY ATOMIC LAYER DEPOSITION FOR ENHANCED ELECTROCHEMICAL PERFORMANCE

by

SAI ABHISHEK PALAPARTY

A THESIS

Presented to the Faculty of the Graduate School of the

MISSOURI UNIVERSITY OF SCIENCE AND TECHNOLOGY

In Partial Fulfillment of the Requirements for the Degree

MASTER OF SCIENCE IN CHEMICAL ENGINEERING

2016

Approved by

Dr. Xinhua Liang, Advisor
Dr. Amitava Choudhury
Dr. Ali Rownaghi

PUBLICATION THESIS OPTION

This thesis consists of the following one article that has been published:

Paper I, Pages 6-41, “Enhanced cycle life and capacity retention of iron oxide ultrathin film coated SnO_2 nanoparticles at high current densities” has been published in RSC Advances 6(29): 24340-24348, 2016. This thesis follows Journal formatting guidelines.

ABSTRACT

Atomic Layer Deposition is a robust technique used to deposit high quality, conformal, and size-tunable ultrathin films on a substrate. This technique can be used to coat protective films on battery anode and cathode materials for enhanced performance. In the case of cathodes, the ultrathin film provides a protective barrier preventing cationic dissolution. In the case of anodes, the film acts as a supporting matrix reducing strain caused by volume expansions. In these study, we use this technique to coat an optimally thick conductive iron oxide film on tin oxide particles to improve its electrochemical performance at high current densities when tested in a practical voltage window. The conductive nature of the iron oxide film enabled faster kinetics at the interface for Li^+ transfer that enabled improved performance.

ACKNOWLEDGMENTS

I would first like to thank my thesis advisor Dr. Xinhua Liang of the Chemical and Biochemical Engineering department at Missouri S&T. The door to Prof. Liang's office was always open whenever I ran into a trouble spot or had a question about my research or writing. He consistently allowed this paper to be my own work but steered me in the right direction whenever he thought I needed it.

I would also like to acknowledge Dr. Amitava Choudhury and Dr. Ali Rownaghi for serving on my thesis committee, and I am gratefully indebted to their very valuable comments on this thesis.

I really appreciate my research group members for their support, friendship, and inputs. I would like to thank Dr. Rajankumar Patel in particular for his patience in making sure that I learn procedures correctly.

Finally, I must express my very profound gratitude to my parents, to my uncle and aunt for providing me with unfailing support and continuous encouragement throughout my years of study and through the process of researching and writing this thesis. This accomplishment would not have been possible without them. I would also like to dedicate this thesis to my grandfather Mr. A.V.S.R.K. Sarma who has been my role model. Thank you.

TABLE OF CONTENTS

LIST OF FIGURES

LIST OF TABLES

SECTION

1. INTRODUCTION

1.1. LITHIUM-ION BATTERY ANODE MATERIALS

The use of lithium-ion (Li-Ion) batteries is widespread in our daily life in portable electronics, electric vehicles, power tools, and various electric grid applications. This influx into our daily lives has been possible due to Li-Ion battery technology's advantages including ease of portability, high power and energy density, and high energy efficiency. With power and energy demand increasing, there is a need for this technology to push for more energy storage capacity, the higher rate at which this stored energy is delivered and longer battery life. A typical Li-Ion battery is made of a positive and negative terminals or electrodes, which are separated by a thin film polymer membrane (separator) to avoid a short circuit between them. The electrodes and separator are generally soaked in a liquid electrolyte (e.g., $LiPF_6$ dissolved in ethyl carbonate and dimethyl carbonate) to facilitate Li^+ ion transfer. The positive electrode or, cathode typically consists of a lithium transition metal oxide (e.g., $LiCoO_2$) whereas the negative electrode or, anode consists typically of graphite. Once, an external connection is established between the two electrodes, chemical reactions convert chemical energy into electrical energy that flows past this external connection. Figure 1.1 illustrates the typical working of Li-ion battery.

When a Li-Ion battery is charging, Li^+ ions are extracted from the cathode side and travel to the anode through the electrolyte where they get inserted into the anode structure. The supplied energy is used to deliver Li^+ ions from the cathode to anode.

However, in the case of discharging, the reverse happens and electrons move from the anode to cathode in the external connection thereby resulting in useful work.

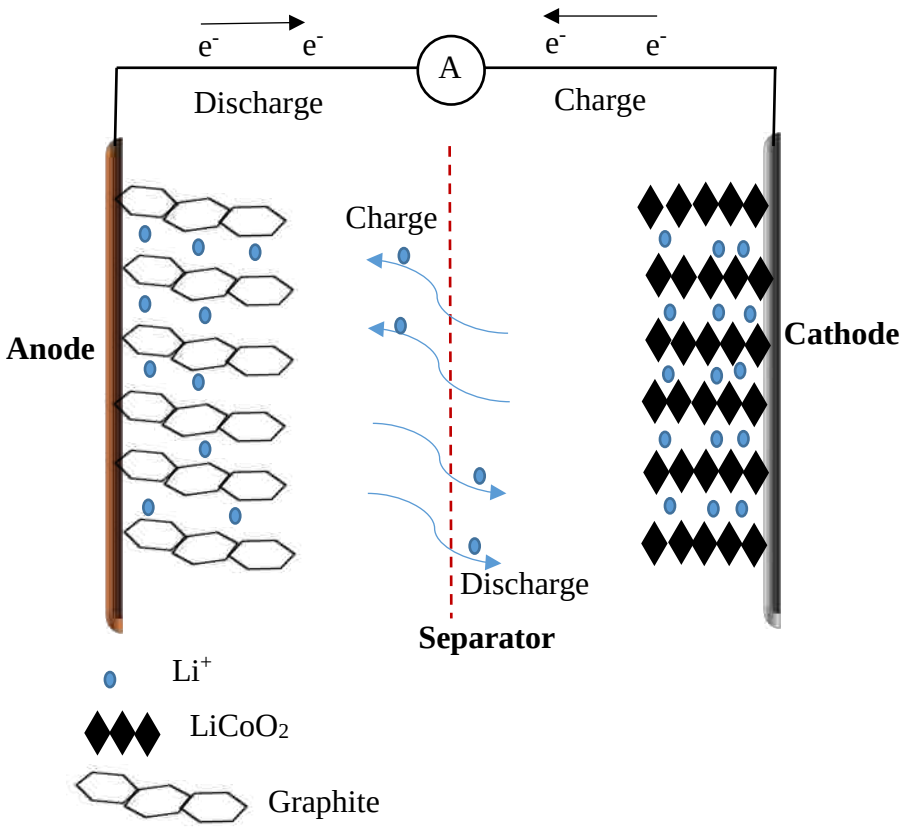

Figure 1.1. An illustration of the charge-discharge process inside a Lithium-Ion battery with $LiCoO_2$ as cathode and graphite as anode

Commercial lithium ion batteries prefer graphite or carbon as an anode material even though it was introduced more than 20 years ago.[1] The intercalation of Li^+ between graphene planes enables electrochemical activity in these materials. When this occurs, volume expansions occur, which can lead to exfoliation of graphite. Also, this results in a strain that can cause damage to SEI layer, thus reducing cell life. With the demand for higher energy density materials, new anode materials have been studied which have a

theoretical capacity much greater than that of graphite (~372 mAh/g). Tin oxide (SnO_2) is one of such materials and has the potential to be commercialized owing to its natural abundance, low cost, and low environmental impact.[2] SnO_2 has a theoretical capacity almost twice as that of graphite (~782 mAh/g). The electrochemical activity in SnO_2 is a result of conversion reaction followed by an alloying reaction as follows:[3, 4]

$$SnO_2 + 2Li^+ + 2e^- \longrightarrow SnO + Li_2O \quad (1)$$

$$SnO + 2Li^+ + 2e^- \longrightarrow Sn + Li_2O \quad (2)$$

$$Sn + xLi^+ + xe^- \longleftrightarrow Li_xSn\ (0 \leq x \leq 4.4) \quad (3)$$

Due to the alloying reaction, SnO_2 experiences huge volume changes, which lead to loss of electrical contacts that cause a reduction in delivered capacity. Also, this is the reason why SnO_2 fails when cycled at high current densities or for a large number of charge-discharge cycles. In this work, an effort was made to improve the performance and life cycle of SnO_2 at high current densities at both room temperature and high temperature (i.e., 55°C).

1.2. ATOMIC LAYER DEPOSITION TECHNIQUE

Atomic layer deposition technique (ALD) can deposits robust, conformal, pin-hole free, and size-tunable films on a substrate. The alternate dosing of precursors enables size tunability, which sets it apart from others deposition techniques such as chemical vapor deposition (CVD) and physical vapor deposition (PVD).[5] The alternate dosing enables self-limiting surface reactions that drive the ALD process. In a typical ALD process, the reactor system is under very low pressure and one of the precursors is introduced into the reaction chamber where the substrate is already present. After some

time, the self-limiting surface reaction saturates the surface and then, the excess precursors and gaseous products are purged and the chamber is flushed using an inert gas. Then the second precursor is introduced and the same process is repeated. This completes one cycle of the ALD process, which results in the deposition of one monolayer. Figure 1.2 illustrates this process for a typical alumina ALD process.

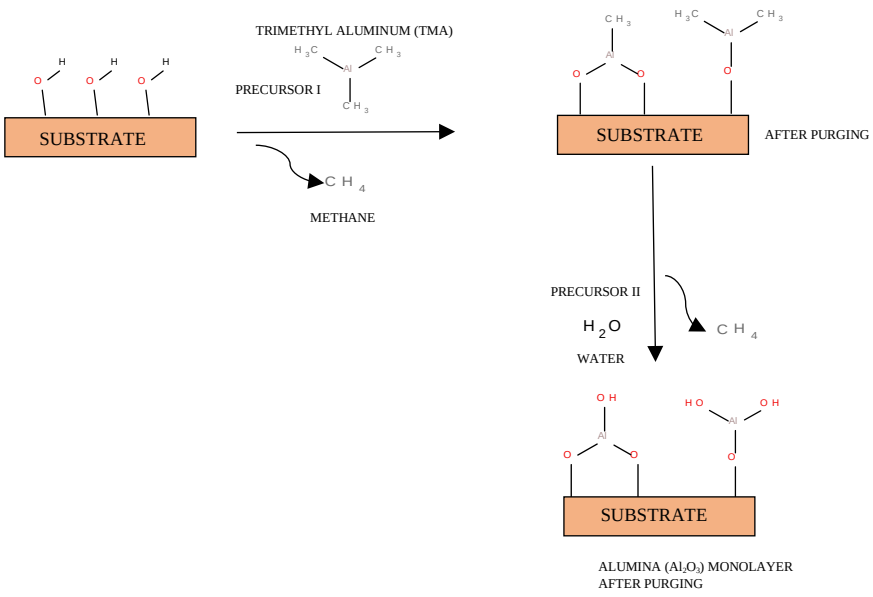

Figure 1.2. A typical alumina ALD process using trimethylaluminum and water as precursors

These advantages of ALD technique have made it a process of choice for coating ultrathin films on lithium ion battery materials that improve their electrochemical performance.[6] ALD films have been coated on various cathode materials such as $LiCoO_2$,[7-9] $LiMn_2O_4$,[10-12] and $LiMn_{1.5}Ni_{0.5}O_4$[13-15] for protection from undesirable reactions with the electrolyte thereby preventing dissolution. ALD coatings have been also used to increase the conductivity of the cathode materials.[12, 16] In present times, ALD coating have been used on next-generation Nickel Manganese Cobalt (NMC) and Nickel

Cathode Aluminum (NCA) cathodes for mitigation of high voltage phase transitions.[17] In the case of anode materials, such as $Li_4Ti_5O_{12}$[18], Si[19, 20], and SnO_2,[21, 22] ALD films were used to buffer volume expansions that improved their electrochemical performance. In this study, iron oxide films were coated on SnO_2 particles by ALD to improve its electrochemical performance. Iron oxide was chosen, since iron oxide is electrochemically active and has been used as an anode with a theoretical capacity higher than that of SnO_2.

PAPER

I. Enhanced Cycle Life and Capacity Retention of Iron Oxide Ultrathin Film Coated SnO_2 Nanoparticles at High Current Densities

Sai Abhishek Palaparty[†], Rajankumar L. Patel[†], Xinhua Liang[*]

Department of Chemical and Biochemical Engineering, Missouri University of Science and Technology, Rolla, MO 65409, USA

[†] These authors contributed equally.

[*] Corresponding author, Email: liangxin@mst.edu

Abstract

Tin oxide (SnO_2) has a high theoretical capacity (~782 mAh/g) but, it experiences large volume changes during charge and discharge cycles that cause rapid capacity fade, which limits its practical use as an anode material. In an attempt to solve this, we coated these particles with ultrathin electrochemically active iron oxide (FeO_x) films that act as an artificial solid electrolyte interphase layer, thus stabilizing the SnO_2 particles for better longevity of significantly improved performance at high current densities in a practical voltage window. Since there exists a tradeoff between species transport and protection of particles (expecting long life), a film with an optimum thickness was achieved by atomic layer deposition (ALD) of FeO_x on SnO_2 particles. With an optimum thickness of about 0.24 nm after 20 cycles of iron oxide ALD (20Fe), an initial capacity of ~ 658 mAh/g was achieved at a high current density of 1,250 mA/g. After 1,000 cycles of

charge/discharge at 1,250 mA/g, the 20Fe sample showed a capacity retention of 94% as compared to 52% of the uncoated sample when cycled at room temperature; at 55 $^{\circ}$C, the capacity retention of the 20Fe sample was 93% compared to 33% of the uncoated sample.

1. Introduction

In recent times, there has been a thrust for improving battery electrode materials for use in applications that require high energy densities, long cycle life and high capacity retention. Traditional lithium ion batteries use graphite as anode material however, drawbacks include exfoliation and sensitivity to electrolyte that reduces its electrochemical performance. Several researchers have focused on using graphene as an alternative to graphite as it delivers better capacity and performance.[1-3] However, the downside of using graphene is that its synthesis process is either complex or expensive. Other materials like $Li_4Ti_5O_{12}$ and TiO_2 have been investigated as alternative anode materials, but they deliver lower capacity than graphite.[4, 5] Tin oxide (SnO_2) has gained significant interest as an alternative to graphite as an anode material in lithium ion batteries (LIBs) due to its high theoretical capacity (~782 $mAhg^{-1}$),[6-9] which is approximately twice that of graphite (~372 $mAhg^{-1}$).[10] SnO_2 is an ideal choice for LIB anodes owing to its natural abundance, low cost, and low environmental impact. However, it has yet to be commercialized because of its low cycleablity due to high volume variations (~250 %) that cause pulverization leading to loss of electrical contacts.[11, 12] Many researchers have tried to use nanostructured particles to alleviate strain that causes these volume expansions.[13-16] However, preparation of such ultra-small nanoparticles may not be commercially viable due to increased costs even though they show improvement in electrochemical performance. Another tactic is to provide a supporting matrix for the SnO_2 particles in form of thin film coating.[17-20] Reported studies of thin film coating mainly focused on liquid phase wet methods. However, these methods have some limitations, leading to poor endurance of electrochemical

performance due to non-uniform (non-conformal) or an excessively thick coating.[21] On the contrary, an ultrathin film with a nanometer or sub-nanometer level thickness has demonstrated to induce stability and enhance electrochemical performance in battery electrode materials.[22-25]

Atomic layer deposition (ALD) is the process of choice for such ultrathin film growth as it enables conformal, pin-hole free, and high aspect ratio film formation.[26] These ultrathin ALD films increased the cycle life and capacity retention; however, normally there was a decrease in the initial discharge capacity of the ALD coated samples, as compared to the uncoated sample. In these studies, an ultra-thin film was generally used and the charge/discharge cycle were limited to small cycle numbers (<200 cycles). This can be due to the fact that these films (e.g., Al_2O_3, ZnO and ZrO_2) used in these studies were insulating and thus increased mass transfer resistance for Li^+ transfer. There was a trade-off between capacity and cycling life due to the insulating properties of ALD films. Recently, we demonstrated that this dilemma could be solved by using conductive ultrathin cerium oxide films.[27] The initial capacity of the optimal 3 nm CeO_2-coated $LiMn_2O_4$ particles showed an initial discharge capacity increase of 24% compared to the pristine one, and the capacity retention significantly improved to 96% and 95% after 1,000 cycles at room temperature and 55 $^{\circ}$C, respectively, when cycled at 1 C rate. This study showed that both high capacity and high cycling stability can be achieved by using suitable conductive thin film coating with an optimal thickness.

In this study, ultrathin iron oxide film is considered as a candidate to improve the performance of SnO_2 nanoparticles, since iron oxide is electrochemically active and has been used as an anode with a theoretical capacity higher than that of SnO_2.[28-30] Also, iron

oxide is abundant in nature and is environmentally benign. Iron oxide thin film coating on SnO_2 has been studied previously and it was found out that the synergy between iron oxide and SnO_2 could stabilize its structure and improve its electrochemical performance.[17, 20, 31-33] However, in these studies, the iron oxide films were prepared by liquid phase methods, and they were either too thick or not conformally coated on the SnO_2 particles surface. In addition, these studies were limited to low cycle numbers of charge/discharge testing or tested at low current densities for capacity retention and/or cycle life. To the best of our knowledge, there has been no electrochemical study of ultrathin film of iron oxide coated on LIB electrode particles by ALD. In this study, we report the initial discharge capacity increase and long cycling life of the iron oxide ALD coated commercial SnO_2 nanoparticles at both room temperature and elevated temperature when tested in a practical voltage window.

2. Experimental

A fluidized bed reactor, as described in detail elsewhere[34] was used to perform ultrathin film coating of iron oxide on as-purchased SnO_2 particles (<100 nm, Aldrich) by ALD. Ferrocene ($C_{10}H_{10}Fe$, 99%, Alfa Aesar) and oxygen gas were used as the precursors for the iron oxide ALD. The reaction temperature was 450 $^{\circ}$C. The reactor was operated at a low pressure of ~5 torr and the quality of fluidization was improved using two vibro motors. The vapor of solid precursor (ferrocene) was sent into the reactor by using a heating bubbler at a pressure of similar order of that of the system. The gas flow rates were controlled using MKS flow controllers. To avoid accumulation of ferrocene on the internal walls of the system and to prevent undesirable CVD (chemical vapor deposition)

reactions, the feed lines were maintained at ~150 °C. The ALD coating process was similar to that applied in our recent publication.[27]

The particles were subjected to X-ray powder diffraction analysis in Philips X-Pert Multi-purpose Diffractometer (MPD) using Cu Kα radiation (λ= 1.54056 Å) with 2θ ranging from 5 to 90° at a scanning rate of 1.4°/min. The coated particles were visualized using FEI Tecnai F20 TEM/STEM supported with an energy dispersive X-ray spectrometer system. The loading of Fe on coated samples was determined using inductively coupled plasma atomic emission spectrometer (ICP-AES). The thermogravimetric analysis (TGA) of the uncoated and the coated particles was conducted using a Q50 TGA/DSC (TA instruments) with a flowing oxygen atmosphere (40 mL/min) at a heating rate of 10°C /min up to 1,000°C.

The anode for the coin cell was prepared using 5 wt. % of PVDF binder dissolved in NMP, which was added to a mixture of 85 wt. % of anode material and 10 wt. % carbon black to form a slurry. Using a razor blade, this slurry was spread on a Cu foil (>99.9%, MTI corporation) uniformly mounted on a glass plate. This electrode composite was placed in an oven and dried under vacuum at 120 °C to evaporate the solvent for 8 hours. After that, disks of approximately 8-13 mm in diameter were punched and cold pressed. Two electrode CR 2032 coin cells were fabricated in an Ar glovebox using punched disks as active anode electrode and with Li metal (99.99%, Aldrich) as counter and reference electrode. The two electrodes were separated using a porous Celgard-2320 separator composed of a 20 μm thick polypropylene (PP)/polyethylene/PP tri-layer film. Commercial electrolyte ($LiPF_6$ in 1:1:1 volume ratio of EC: DMC: DEC) was used as purchased from MTI corporation.

The prepared CR 2032 coin cells were subjected to galvanostatic charge-discharge capacity testing at different current densities, capacity retention testing for 1,000 charge-discharge cycles and ac impedance analysis at room temperature as well as at 55 $^{\circ}$C. An 8-channel battery analyzer (Neware Corporation) was used to measure charge/discharge capacity ranging from 0.5 to 3 V. Electrochemical impedance spectroscopy (EIS) of the prepared cells were performed using a BioLogic SP-150 potentiostat and impedance analyzer. The impedance was measured over a frequency range of 0.01Hz - 1MHz and at a perturbation of 5 mV. Equivalent circuit models for the impedance spectra were fitted using EC-Lab software.

3. Results and Discussion

Different thicknesses of iron oxide films were coated on SnO_2 nanoparticles by ALD. In an attempt to find an optimal thickness of iron oxide films on SnO_2 particles, the particles were coated with 10 cycles (10Fe), 15 cycles (15Fe), 20 cycles (20Fe), 30 cycles (30Fe), and 100 cycles (100Fe) of iron oxide films. XRD analysis was performed on the 30Fe and 100Fe samples to determine the phase of iron oxide ALD films deposited on the SnO_2 particles. In this study, the phase of the iron oxide in the ultrathin film cannot be interpreted without ambiguity (see Figure S1 in Electronic Supplementary Information). The TGA results were also inconclusive about the phase of iron oxide deposited by ALD on the SnO_2 particles (see Figure 2 in Electronic Supplementary Information). Henceforth, it is referred as FeO_x in the paper. Transmission electron microscopy (TEM) images of the 30Fe and the 100Fe samples are shown in Figure 1. In Figure 1a, the film on the 30Fe sample cannot be seen clearly, since the film is very thin, but energy

dispersive spectroscopy (EDS) spectrum of the 30Fe sample clearly indicates significant peaks for Fe, which confirm the presence of iron in the sample (see Figure S3a in Electronic Supplementary Information). For the 100Fe sample, a conformal film of ~1.2 nm can be seen clearly (Figure 1b). Conformity is one of the characteristics of the ALD coating process.[26, 27] The EDS spectrum of the 100Fe sample (see Figure S3b in Electronic Supplementary Information) shows stronger peaks for Fe as compared to the 30Fe sample, since there was more FeO_x loading with the increase in the number of ALD cycles. The growth rate of FeO_x ALD film is estimated to be ~ 0.012 nm/cycle based on the TEM image of the 100Fe sample in this work. This growth rate is in good agreement with the results of previous studies of iron oxide film growth by ALD using ferrocene and oxygen as precursors.[35] Brunauer–Emmett–Teller (BET) isotherms were obtained for the 30Fe sample using Quantachrome Autosorb-1. The surface area of the 30Fe sample was found to be 33.5 m^2/g. Based on the surface area, assuming the iron oxide phase in the ultrathin film to be Fe_2O_3, and the percentage of Fe on the sample obtained from inductively coupled plasma atomic emission spectroscopy (ICP-AES) (see Figure S4 in Electronic Supplementary Information), the expected thickness of the ultrathin film was found to be about 0.4 nm, which is very close to the thickness of 0.36 nm based on the growth rate of 0.012 nm/cycle.

Figure 2 depicts the galvanostatic discharge capacities of coin cells assembled from the UC, 10Fe, 15Fe, 20Fe, and 30Fe samples obtained using different current densities at both room temperature and 55 $^{\circ}C$. The measurements were carried out at different current densities of 50 mA/g, 125 mA/g, 250 mA/g, 500 mA/g, 1,250 mA/g, and 2,500 mA/g and each for five cycles. In this study, we used the discharge cutoff voltage

to 0.5 V as a practical limit and the charge cutoff voltage to 3 V for testing the cycle life and capacity retention of our coated and uncoated samples. Cycling at room temperature and a low current density of 50 mA/g, the UC sample showed a discharge capacity of ~744 mAh/g, which is close to the theoretical capacity of SnO_2. The 10Fe, 15Fe and 20Fe exhibited higher initial discharge capacities as compared to the UC and the 30Fe sample at the current densities of 50 mA/g, 125 mA/g, and 250 mA/g. At high current densities (i.e., 1,250 mA/g), a clear distinction is seen in the performance of various samples. The UC sample performed poorest due to formation of solid electrolyte interface (SEI) at high current densities. The 10Fe, 15Fe, and 20Fe performed significantly well in terms of capacity retention as the ultrathin coating served as an artificial SEI layer at higher current densities. However, the 30Fe sample performed the poorest among the coated samples. A similar trend was observed at 55 $^{\circ}$C; however, the initial capacities of the 10Fe, 15Fe, and 20Fe samples at the low current density of 50 mA/g were higher than those tested at room temperature. This could be resulted from high electrical and ionic conductivity, and low ohmic potential at high temperature for tin based electrodes.[36]

The SEI is very crucial for the cycle life of the LIB.[37] This is because it forms a protective layer that prevents undesirable reactions with the electrolyte, but it grows thicker while cycling, which eventually slows the Li^+ diffusion. Therefore, the ultrathin ALD film in our case can act as an artificial SEI layer thereby passivating the entire surface of the active material, and potentially stopping the formation of the growing organic SEI layer. This could be the reason for better performance of the coated samples as compared to the UC sample during cycling at high current densities of 1,250 mA/g and 2,500 mA/g. Most of the previous ALD studies on battery electrode particles

demonstrated that this ultrathin coating could delay the transport of Li^+, thus decreasing the specific capacity.[21, 27] The reason is that the ALD films were insulating metal oxides in the previous studies. In this study, iron oxide was used as the coating materials. Iron oxide is electrochemically active and has been used as anode materials. In addition, iron oxide has a higher theoretical specific capacity as compared to tin oxide.[29, 30] At a low current density of 50 mA/g, the 10Fe, 15Fe and 20Fe samples showed an improvement in initial capacity both at room temperature and at 55 $^{\circ}$C, when compared to the UC sample. This trend of increase in initial discharge capacity at higher temperature is in agreement with other studies on iron oxide/SnO_2 nanocomposites.[38, 39] The voltage testing window falls inside the electrochemical active region for iron oxide. This means elemental Fe was formed due to irreversible initial reaction between iron oxide and Li^+. The reaction between SnO_2 and Li^+ yielded Sn and Li_2O. This means there would be formation of Sn/Fe/Li_2O matrix. The formation of Sn/Fe/Li_2O matrix further increased the electronic conductivity.[17] In one previous report of graphene/SnO_2/Fe_2O_3 nanocomposites, the Sn acted as an inactive matrix for the iron oxide, which contributed most towards capacity.[39] However, in our case, the film is very thin and the amount of iron oxide is very less than that of the SnO_2. Hence, it is very difficult to determine individual contribution of SnO_2 and iron oxide towards the capacity of the coated samples.

The exact reason for the poor performance of the 30Fe sample is not clear. This could be due to the increased mass transfer resistance of Li^+ due to “excessive” thickness of the film. Similar thickness effect was observed for the case of $LiMn_2O_4$ particles coated with CeO_2 films.[27] However, 30 cycles of iron oxide is only about 0.36 nm thick (growth rate of 0.012 nm/cycle), which may seem too thin to be said excessively thick.

For example, in our recent studies, the optimum thickness of CeO_2 films on 8 μm $LiMn_2O_4$ particles was 3 nm.[27] Studies by Lee et al. showed that a 1.1 nm thick alumina coating on $LiCoO_2$ (~400 nm) itself was too thick and increased Li^+ diffusion resistance.[40] Studies by Guan and Wang of alumina ALD coated on micron sized $LiMn_2O_4$ powders showed that a film thickness of ~1.2 nm was too thick.[41] Sun et al. showed that a ~1 nm thick film of ZrO_2 on $Li_4Ti_5O_{12}$ anode had an optimal performance.[42] 1.2 nm alumina is overly thick, while 3 nm of CeO_2 is not, because the alumina film is insulating whereas CeO_2 has high ionic conductivity and has been used as a solid electrolyte.[43, 44] Hence, it can be said that the definition of "overly" thick film depends upon the nature of the film and the substrate.

Herein, the FeO_x film of ~0.36 nm thickness may itself be too thick for the nano-SnO_2 particles in the 30Fe sample. Recent study on lithium ion diffusion mechanism in iron oxide electrode suggested that there existed three regions in the diffusion profile of intercalated iron oxide.[45] The region consisting of Fe/Li_2O was found to be the slowest for Li^+ diffusion. In our case, the Li^+ ion first reacted with the FeO_x film before entering the SnO_2 lattice and hence, $Fe/Sn/Li_2O$ matrix would form. With increase in the number of ALD coating cycles, the FeO_x film got thicker, which in turn lead to more Fe/Li_2O formation. Since, this is the region for the slowest diffusion for Li^+, and with limited lithiation, it increased the mass transfer resistance in case of 30Fe sample that led to poorer performance as compared to the other coated samples at higher current densities. Hence, it can be said that the 30Fe sample has an "overly" thick ALD film. Studies to understand this mechanism in detail is being pursued.

To see whether this ALD coating enhances the electrochemical performance in terms of capacity retention and cycle life of SnO_2 at higher current densities, the samples were cycled at a high current density of 1,250 mA/g at both room temperature and at 55 $^{\circ}$C (Figure 3). The FeO_x coated samples (10Fe, 15Fe, and 20Fe) performed far better in terms of capacity retention. At room temperature, after 1,000 cycles of charge/discharge, the coated samples showed high capacity retention, ~91% capacity retention of the 10Fe sample, ~92% of the 15Fe sample, and ~94% of the 20Fe sample. This is because the ultrathin film was sufficiently thick and provided artificial SEI. Also, the formation of the electronic conductive in-situ Sn/Fe/Li_2O matrix leads to a better capacity as compared to the UC sample even after a large number of charge-discharge cycles. In contrast, the 30Fe, similar as the UC, experienced a severe capacity fade after only 350 cycles as compared to the other coated samples at room temperature. At room temperature after 1,000 cycles, the capacity retention of the UC sample was about ~52%. The performance of 30Fe sample is even worse as it showed a capacity retention of only ~11% after 1,000 cycles at this current density. This is because of the formation of thick SEI on the UC sample and the presence of "overly" thick FeO_x film on the 30Fe sample.

At 55 $^{\circ}$C, a similar trend was observed but there was an increase in initial discharge capacity of the coated samples when compared to the testing at room temperature. The 10Fe sample showed a capacity retention of ~89%, compared to ~90% of the 15Fe sample and ~93% of the 20Fe sample after 1,000 charge/discharge cycles. The very high capacity retention over long cycling of these coated samples can be attributed to the formation of the stable artificial SEI layer provided by the ultrathin film. At higher temperature, the performance of the cell degrades faster.[46] This is also

evidenced in form of reduced capacity retention during testing at higher temperature. The capacity retention of the UC and 30Fe sample at this temperature is ~33% and ~10%, respectively.

To further understand the effect of this ultrathin film on the performance of the SnO_2 particles, testing was performed at lower current densities at both room temperature and 55 $^{\circ}$C. Figure 4 shows the results at a current density of 500 mA/g. The UC sample showed an initial discharge capacity of ~680 mA/g at room temperature. The 10Fe, 15Fe and 20Fe samples showed an initial discharge capacity of ~689 mAh/g, ~706 mAh/g and ~720 mAh/g, respectively, at room temperature. The 10Fe, 15Fe and 20Fe samples showed excellent capacity retention of ~ 93%, ~ 93%, ~ 94%, respectively, even after 1,000 cycles. With decrease in current density, there was more capacity retention for the UC and the 30Fe sample. The UC sample retained a capacity of ~66%, whereas the 30Fe sample retained a capacity of ~62% after 1,000 cycles. As in the previous case, the initial capacity of the samples further improved and the capacity retention decreased when tested at a higher temperature of 55 $^{\circ}$C.

The cycling performance of the cells were also tested at a current density of 250 mA/g at both room temperature and 55 $^{\circ}$C (see Figure S5 in Electronic Supplementary Information). Compared to the testing at 500 mA/g, all the samples showed a further improvement in capacity retention at both room temperature and 55 $^{\circ}$C. These results suggest that the effect of the ultrathin film is more significant for the samples tested at high current densities as it passivated the particle surface by serving as an artificial conformal SEI layer and thus providing protection from undesirable reactions with the electrolyte. It is also interesting to note that during initial cycles, the 30Fe sample

performed better than the UC sample. However, with cycling the 30Fe sample performs poorer as compared to the UC sample (Figures 3 and 4). This could be due to the electrochemical active nature of the ultrathin film. As discussed earlier, when Li^+ reacts with iron oxide, volume expansions occur.[28-30] This could increase the stress on the ultrathin film. This increased stress could be the reason for poorer performance of 30Fe sample than that of the UC sample.

This series of testing indicates that the 10Fe, 15Fe, and 20Fe samples showed a very high capacity retention even after 1,000 cycles of charge/discharge at a high current density of 1,250 mA/g. This is a significant achievement as compared to the previous studies. For example, FeO_x/SnO_2 composite synthesized by El-Shinawi et al. showed a capacity retention of only ~20% after 100 cycles when discharged at a current density of 400 mA/g.[17] Heterostructures of iron oxide and SnO_2 produced by Zhou et al. also showed significant capacity fade of about 75% only after 30 charge/discharge cycles at 1,000 mA/g.[32] In contrast, our 20Fe sample showed a significantly higher capacity retention of 94% even at a high current density of 1,250 mA/g after 1,000 cycles at room temperature. Ultra-small SnO_2 nanocomposites have demonstrated enhanced performance in terms of capacity retention at high current densities.[7, 16] However, the average size of the synthesized particles in these studies was less than <10 nm. Our study is unique as we demonstrated how capacity retention can be improved for much larger commercial SnO_2 nanoparticles (<100 nm) using optimal ultrathin film coating by ALD.

To understand the kinetics change due to the ultrathin film, EIS analysis was performed for the coated samples as well as the uncoated samples at room temperature and 55 $^{\circ}$C. Figure 5 presents the results tested at room temperature. The equivalent circuit

(Figure 5c), comprised of three resistances. R_{ohm} refers to the uncompensated ohmic resistance between the working electrode and the reference electrode, i.e., R_f (the resistance for lithium ion mobility in the surface layer including SEI layer and/or surface modification layer), C_{ct} (the ideal capacitance of the surface layer and the double layer), and R_{ct} (the charge transfer resistance). W represents the Warburg impedance that outlines the lithium ion diffusion in the bulk material. The Warburg impedance and the lithium ion diffusion coefficent of the working electrode are inversely proportional. Though these values of resistances have no physical significance, it can be used to compare the kinetics of the coated and the uncoated samples.

At room temperature, in the EIS of the fresh cells, two significant semicircles for the UC sample, whereas only one major semicircle was observed for the coated samples. In the case of the coated samples, there was overlap between contribution of the charge transfer resistance at mid-high frequencies and the SEI layer/ultrathin coating contribution at high frequencies,[47] which could be the reason for appearance of only one major semicircle in the EIS. From the impedance parameters tested at room temperature (Table 1), the 20Fe sample has the least charge transfer and warburg impedance values, when compared to other samples before and after 1,000 charge/discharge cycles. The coated samples showed low film resistance even after 1,000 cycles of charge/discharge, when compared to the UC sample. Out of all the tested samples, the 30Fe sample shows the highest diffusion resistance, which could be the reason for its poor performance when compared to the other coated samples. As compared to the 30Fe sample, the decreasing values of the charge transfer resistance and lower warburg impedance values of the 10Fe,

15Fe and 20Fe samples served as evidence to say that the 20Fe sample had an optimal fim thickness.

At 55 ºC, a similar trend was seen when compared to the EIS analysis at room temperature. For the coated samples only one semicircle was observed, whereas for the uncoated sample, two semicircles were present in the EIS analysis (Figure 6). Out of all the samples, the 20Fe sample showed the lowest charge transfer resistance and warburg resistance, as compared to the other samples after 1,000 cycles of charge/discharge (Table 2). These values are also lower when compared to the results tested at room temperature. This could be due to the increase in electric and ionic conducitivity of SnO_2 particles at higher temperatures. The 30Fe sample experiences the highest warburg resistance of all the samples. When compared to the room temperature testing, the charge transfer and the warburg resistance values decreased during the testing at 55 ºC. This supplements the improved performance of the coated samples at higher temperatures when compared to the samples tested at room temperature in terms of initial capacity.

From the EIS analysis at both room temperature and at 55 ºC, it is found that the 20Fe sample has the optimal ALD film thickness. Iron oxide is conductive (see Figure S6 in Electronic Supplementary Information). The lower values of the film resistance of the coated samples, as compared to the uncoated sample, after 1,000 cycles of charge/discharge is indicative of the ultrathin film serving as an artificial SEI layer. The lower charge transfer, film and warburg resistances of the 10Fe, 15Fe and 20Fe samples, as compared to the UC sample, could probably explain improved performace at high current densities.

4. Conclusions

This work demonstrates that electrochemically active iron oxide films with an optimal thickness can significantly improve the life of cycling, and capacity retention of SnO_2 nanoparticles at high current densities when operated in a practical voltage window. From the electrochemical testing data at both room temperature and at 55 ºC, the 20Fe sample had the best performance in terms of capacity retention for long cycle life. At a current density of 1,250 mA/g, the coated samples (10Fe, 15Fe, and 20Fe) exhibited a capacity retention of at least ~90% after 1,000 charge/discharge cycles at room temperature and ~89% at 55 ºC, respectively. In contrast, the capacity retention of the UC sample at these conditions was ~52% and ~33%, respectively. The reason for such improvement can be attributed to the conformal supporting matrix provided by the electrochemically active iron oxide coating and the synergy between iron oxide and SnO_2. The "overly" thick FeO_x film of the 30Fe sample led to poorer performance as compared to the other coated samples. This work demonstrates the importance of ALD as a very promising technique in stabilizing LIB anode particles for improved performance for long cycle life in lithium ion batteries.

Acknowledgements

This work was supported in part by the National Science Foundation grant NSF CBET 1510085. The authors thank Clarissa A. Wisner and Jessica Terbush at the Materials Research Center at Missouri University of Science and Technology for the TEM analysis.

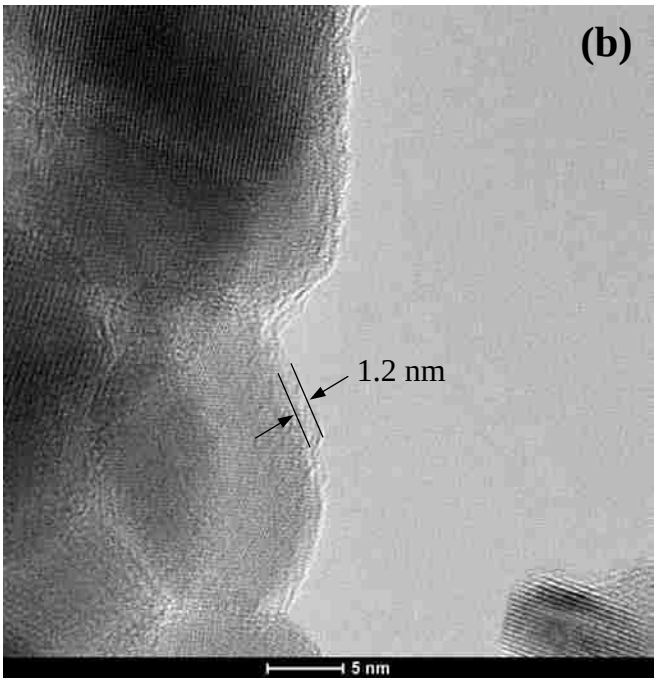

Figure 1. TEM images (a) 30 cycles and (b) 100 cycles of iron oxide ALD coated SnO_2 nanoparticles

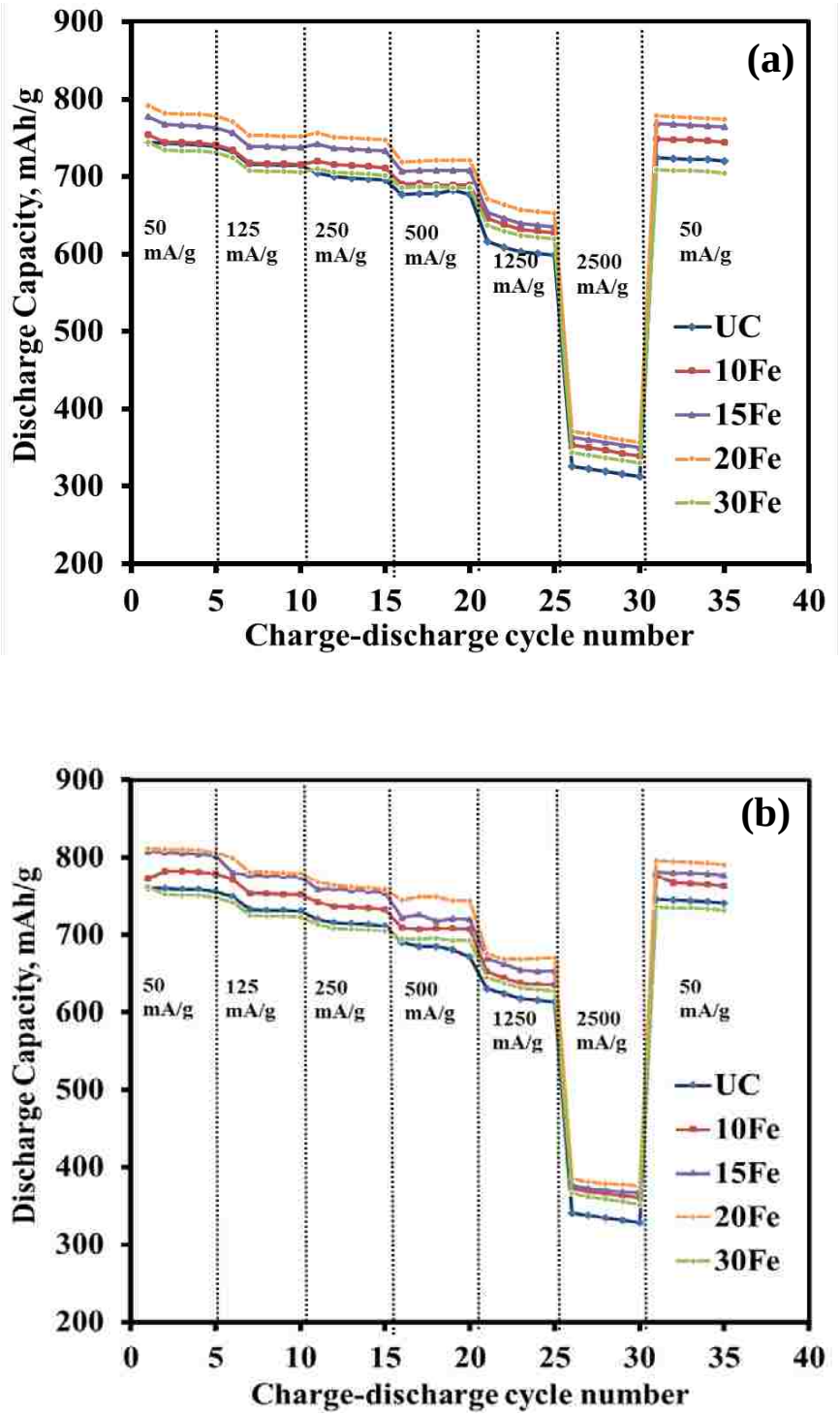

Figure 2. Galvanostatic discharge capacities at different current densities of SnO_2 particles coated with various thicknesses of iron oxide ALD films between 0.5-3V at (a) room temperature and (b) 55 $^{\circ}$C

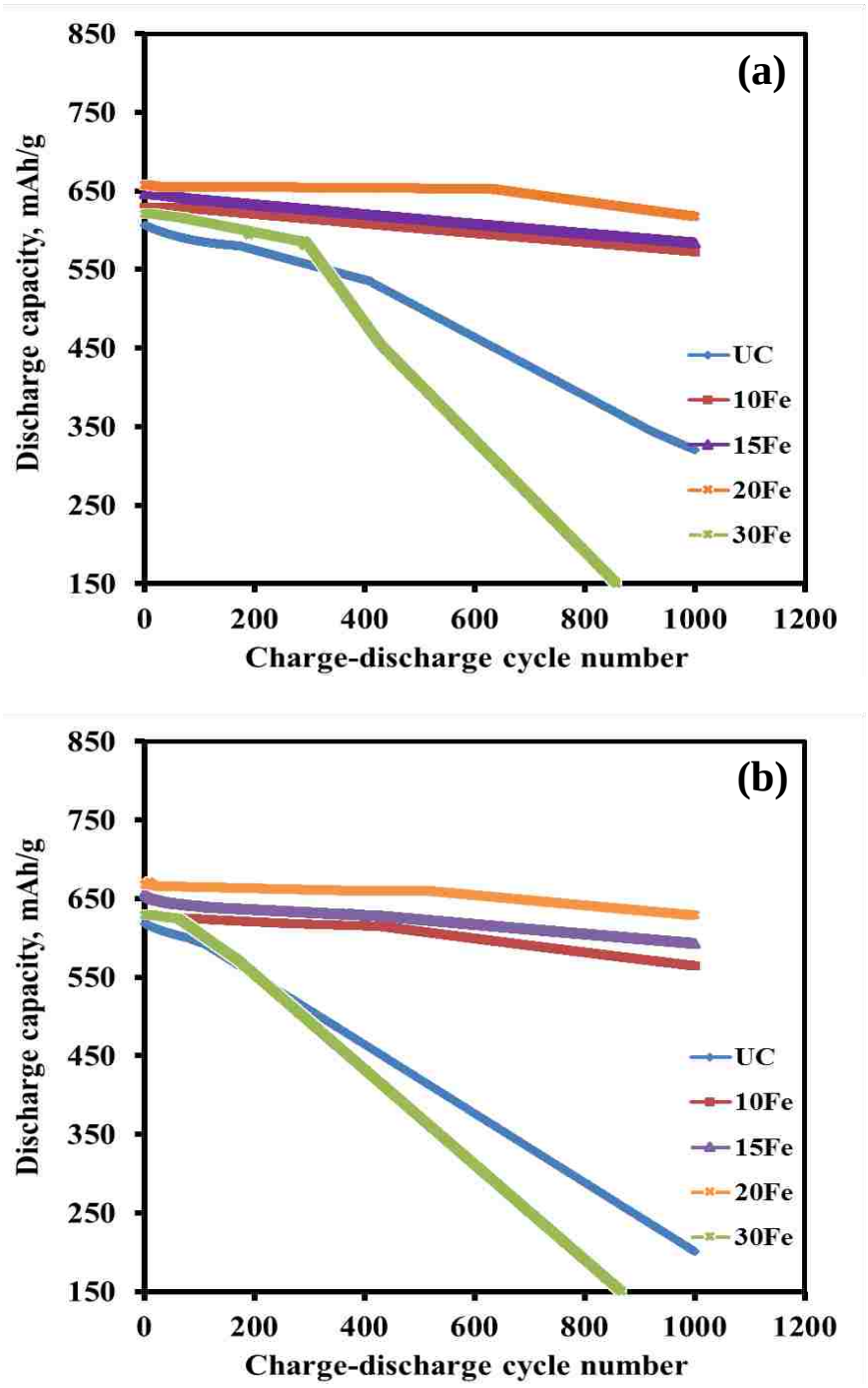

Figure 3. Galvanostatic discharge capacities of SnO_2 particles coated with various thicknesses of iron oxide ALD films at 1,250 mA/g between 0.5-3V at (a) room temperature (b) 55 $^{\circ}$C

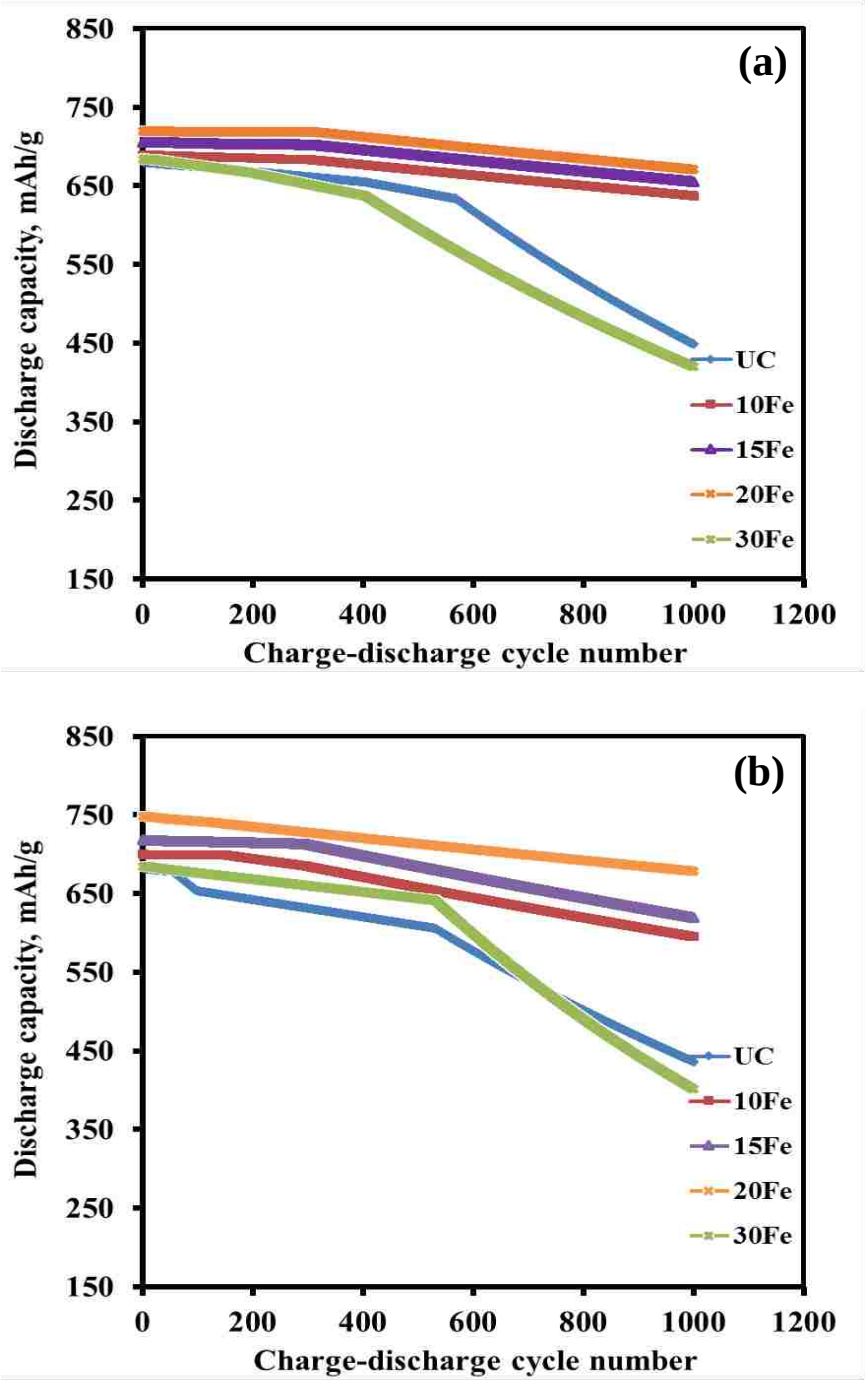

Figure 4. Galvanostatic discharge capacities of SnO_2 particles coated with various thicknesses of iron oxide ALD films at 500 mA/g between 0.5-3V at (a) room temperature (b) 55 $^{\circ}$C

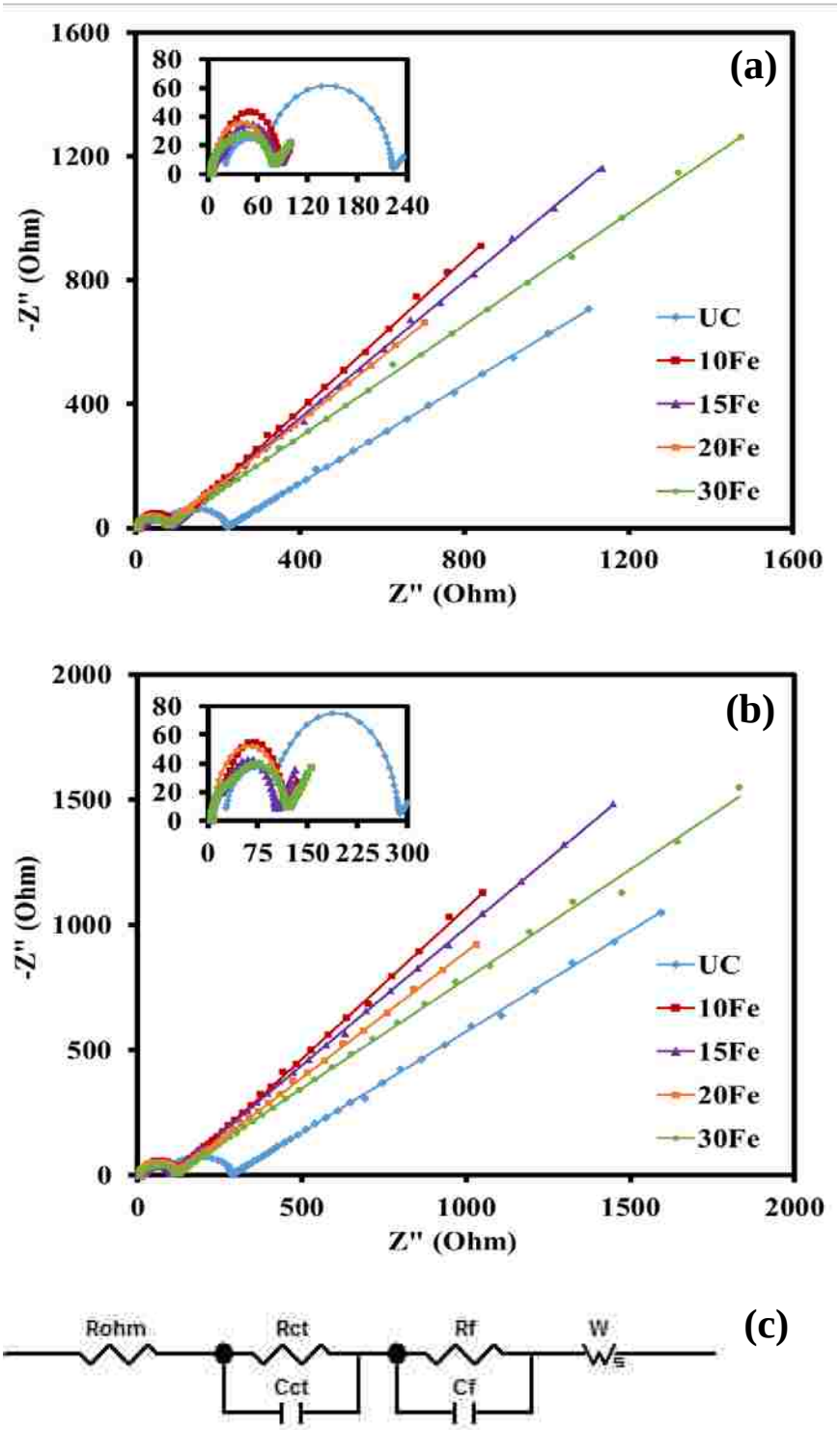

Figure 5. Electrochemical impedance spectra for uncoated and SnO_2 particles coated with various thicknesses of iron oxide with (a) 0^{th} cycle and (b) $1{,}000^{th}$ cycle at room temperature, and (c) equivalent circuit used for fitting electrochemical impedance spectra. Inset shows the higher frequency (10 MHz-1 Hz) semi-circle region

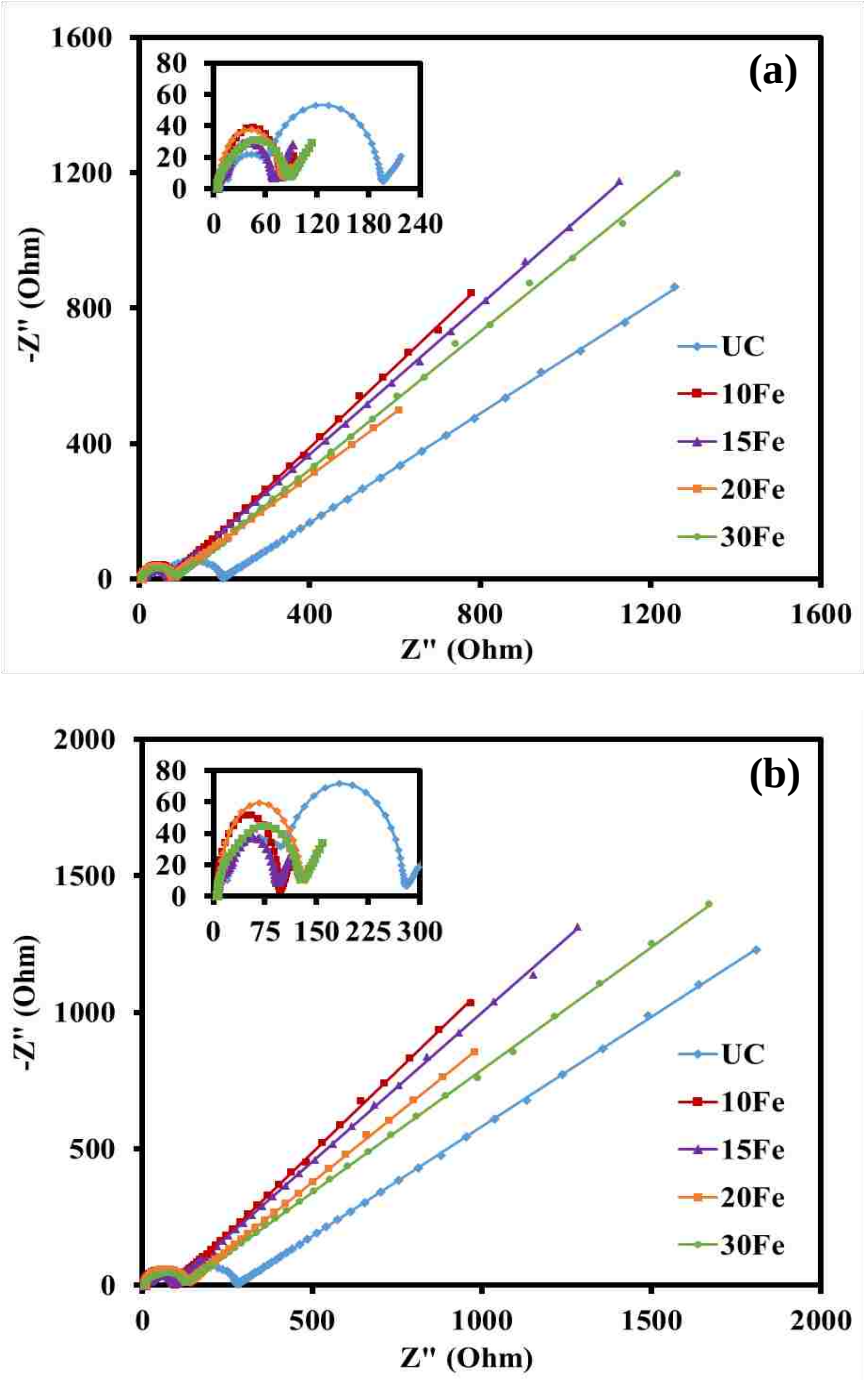

Figure 6. Electrochemical impedance spectra for uncoated and SnO_2 particles coated with various thicknesses of iron oxide with (a) 0^{th} cycle and (b) $1{,}000^{th}$ cycle at 55 $^{\circ}$C. Inset shows the higher frequency (10MHz-1Hz) semi-circle region

Table 1. Impedance parameters using equivalent circuit for EIS spectra at room temperature

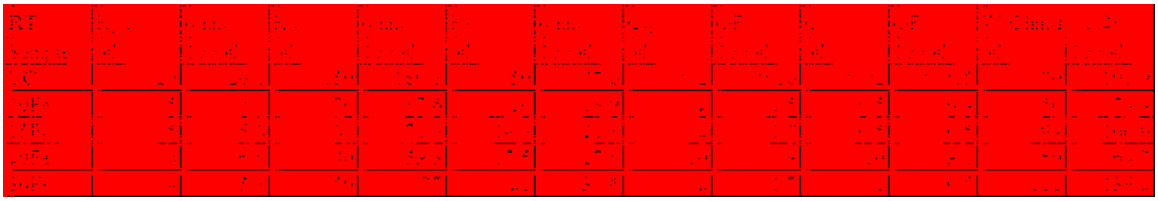

Table 2. Impedance parameters using equivalent circuit for EIS spectra at 55 ºC

55 °C	R_{ohm}	(ohm)	R_{ct}	(ohm)	R_f	(ohm)	C_{ct}	(µF)	C_f	(µF)	W(Ohm.s^-1/2)	
Sample	0th	1000th	0th	1000th	0th	1000th	0th	1000th	0th	1000th	0th	1000th
UC	15	19.2	130	172.7	13	47.3	0.3	0.21	0.022	0.013	84.3	121.7
10Fe	5	6.3	63.2	73.6	7.8	15.3	2.1	0.18	0.5	0.4	55.7	69.3
15Fe	4.8	6	51.2	64.2	10	18.3	2.3	2.1	0.6	0.5	84	94.7
20Fe	5.5	7	32	60.1	12.1	22.8	12	9	11.5	10	42.3	67.8
30Fe	4.3	6	62	88	15.3	27.1	2.1	1.9	1.2	1	105.3	122.9

References

1. P. Lian, X. Zhu, S. Liang, Z. Li, W. Yang and H. Wang, Electrochimica Acta, 2010, 55, 3909-3914.

2. G. Wang, X. Shen, J. Yao and J. Park, Carbon, 2009, 47, 2049-2053.

3. Q. Etienne, R. Frédéric, E. Fabrice, F. Pascal, K. Emmanuel, V. George, G. Feliciano, M.-G. Beatriz, M. Iwan, G. Selmiye Alkan, Y. Ayşe Bayrakçeken, N. Vito Di, T. Alexandr, B. Igor, T. Diana, S. Gotthard, C. Luigi, S. Giorgio, T. Valentina, B. Paolo, P. Grégory, B. Cristina, C. Daniel, S. Gurpreet, R. Teófilo, K. Gunwoo, Y. Wanjing, P. G. Clare and P. Vittorio, 2D Materials, 2015, 2, 030204.

4. X. Sun, M. Hegde, Y. Zhang, M. He, L. Gu, Y. Wang, J. Shu, P. V. Radovanovic and B. Cui, International Journal of Electrochemical Science, 2014, 9, 1583-1596.

5. Y. Ren, Z. Liu, F. Pourpoint, A. R. Armstrong, C. P. Grey and P. G. Bruce, Angewandte Chemie International Edition, 2012, 51, 2164-2167.

6. A. Gildea, D. Wang and G. Botte, Journal of Applied Electrochemistry, 2015, 45, 217-224.

7. L. Liu, M. An, P. Yang and J. Zhang, Scientific Reports, 2015, 5, 9055.

8. A. K. Rai, L. T. Anh, J. Gim, V. Mathew and J. Kim, Electrochimica Acta, 2013, 109, 461-467.

9. M. Winter and J. O. Besenhard, Electrochimica Acta, 1999, 45, 31-50.

10. H. Buqa, D. Goers, M. Holzapfel, M. E. Spahr and P. Novák, Journal of The Electrochemical Society, 2005, 152, A474-A481.

11. D. Ahn, X. Xiao, Y. Li, A. K. Sachdev, H. W. Park, A. Yu and Z. Chen, Journal of Power Sources, 2012, 212, 66-72.

12. I. A. Courtney and J. R. Dahn, Journal of The Electrochemical Society, 1997, 144, 2943-2948.

13. Y. Han, X. Wu, Y. Ma, L. Gong, F. Qu and H. Fan, CrystEngComm, 2011, 13, 3506-3510.

14. J. Hassoun, G. Derrien, S. Panero and B. Scrosati, Advanced Materials, 2008, 20, 3169-3175.

15. P. Poizot, S. Laruelle, S. Grugeon, L. Dupont and J. M. Tarascon, Nature, 2000, 407, 496-499.

16. L. Ding, S. He, S. Miao, M. R. Jorgensen, S. Leubner, C. Yan, S. G. Hickey, A. Eychmüller, J. Xu and O. G. Schmidt, Scientific Reports, 2014, 4, 4647.

17. H. El-Shinawi, A. S. Schulze, M. Neumeier, T. Leichtweiß and J. Janek, The Journal of Physical Chemistry C, 2014, 118, 8818-8823.

18. X. Ji, X. Huang, J. Liu, J. Jiang, X. Li, R. Ding, Y. Hu, F. Wu and Q. Li, Nanoscale Res Lett, 2010, 5, 649-653.

19. J. Lin, Z. Peng, C. Xiang, G. Ruan, Z. Yan, D. Natelson and J. M. Tour, ACS Nano, 2013, 7, 6001-6006.

20. Y. Wang, J. Xu, H. Wu, M. Xu, Z. Peng and G. Zheng, Journal of Materials Chemistry, 2012, 22, 21923-21927.

21. Z. Chen, Y. Qin, K. Amine and Y. K. Sun, Journal of Materials Chemistry, 2010, 20, 7606-7612.

22. H.-M. Cheng, F.-M. Wang, J. P. Chu, R. Santhanam, J. Rick and S.-C. Lo, The Journal of Physical Chemistry C, 2012, 116, 7629-7637.

23. X. Meng, X.-Q. Yang and X. Sun, Advanced Materials, 2012, 24, 3589-3615.

24. J. Zhao and Y. Wang, The Journal of Physical Chemistry C, 2012, 116, 11867-11876.

25. Y. S. Jung, A. S. Cavanagh, L. A. Riley, S.-H. Kang, A. C. Dillon, M. D. Groner, S. M. George and S.-H. Lee, Advanced Materials, 2010, 22, 2172-2176.

26. S. M. George, Chemical Reviews, 2010, 110, 111-131.

27. R. L. Patel, H. Xie, J. Park, H. Y. Asl, A. Choudhury and X. Liang, Advanced Materials Interfaces, 2015, 2, 150046.

28. L. Ji, Z. Lin, M. Alcoutlabi and X. Zhang, Energy & Environmental Science, 2011, 4, 2682-2699.

29. Y. NuLi, P. Zhang, Z. Guo and H. Liu, Journal of The Electrochemical Society, 2008, 155, A196-A200.

30. L. Zhang, H. B. Wu and X. W. Lou, Advanced Energy Materials, 2014, 4, 1300958.

31. R. Jin, Y. Guan, H. Liu, J. Zhou and G. Chen, ChemPlusChem, 2014, 79, 1643-1648.

32. W. Zhou, C. Cheng, J. Liu, Y. Y. Tay, J. Jiang, X. Jia, J. Zhang, H. Gong, H. H. Hng, T. Yu and H. J. Fan, Advanced Functional Materials, 2011, 21, 2439-2445.

33. M. M. Rahman, A. M. Glushenkov, T. Ramireddy, T. Tao and Y. Chen, Nanoscale, 2013, 5, 4910-4916.

34. X. Liang, L. F. Hakim, G.-D. Zhan, J. A. McCormick, S. M. George, A. W. Weimer, J. A. Spencer, K. J. Buechler, J. Blackson, C. J. Wood and J. R. Dorgan, Journal of the American Ceramic Society, 2007, 90, 57-63.

35. J. R. Scheffe, A. Francés, D. M. King, X. Liang, B. A. Branch, A. S. Cavanagh, S. M. George and A. W. Weimer, Thin Solid Films, 2009, 517, 1874-1879.

36. G. Kilibarda, S. Schlabach, T. Hanemann and D. Szabó, International Journal of Electrochemical Science, 2013, 8, 6212-6219.

37. M. B. Pinson and M. Z. Bazant, Journal of the Electrochemical Society, 2013, 160, A243-A250.

38. J. S. Chen, C. M. Li, W. W. Zhou, Q. Y. Yan, L. A. Archer and X. W. Lou, Nanoscale, 2009, 1, 280-285.

39. G. Xia, N. Li, D. Li, R. Liu, C. Wang, Q. Li, X. Lü, J. S. Spendelow, J. Zhang and G. Wu, ACS Applied Materials & Interfaces, 2013, 5, 8607-8614.

40. I. D. Scott, Y. S. Jung, A. S. Cavanagh, Y. Yan, A. C. Dillon, S. M. George and S.-H. Lee, Nano Letters, 2011, 11, 414-418.

41. D. Guan and Y. Wang, Ionics, 2013, 19, 1-8.

42. J. Liu, X. Li, M. Cai, R. Li and X. Sun, Electrochimica Acta, 2013, 93, 195-201.

43. K. Eguchi, T. Kunishaki and H. Arai, Journal of the American Ceramic Society, 1986, 69, C282-C285.

44. H. Yahiro, Y. Baba, K. Eguchi and H. Arai, Journal of The Electrochemical Society, 1988, 135, 2077-2080.

45. B. Tian, J. Światowska, V. Maurice, C. Pereira-Nabais, A. Seyeux and P. Marcus, The Journal of Physical Chemistry C, 2015, 119, 919-925.

46. F. Leng, C. M. Tan and M. Pecht, Scientific Reports, 2015, 5, 12967.

47. Z. C. Orel and B. Orel, Journal of Materials Science, 1995, 30, 2284-2290.

Supporting Information

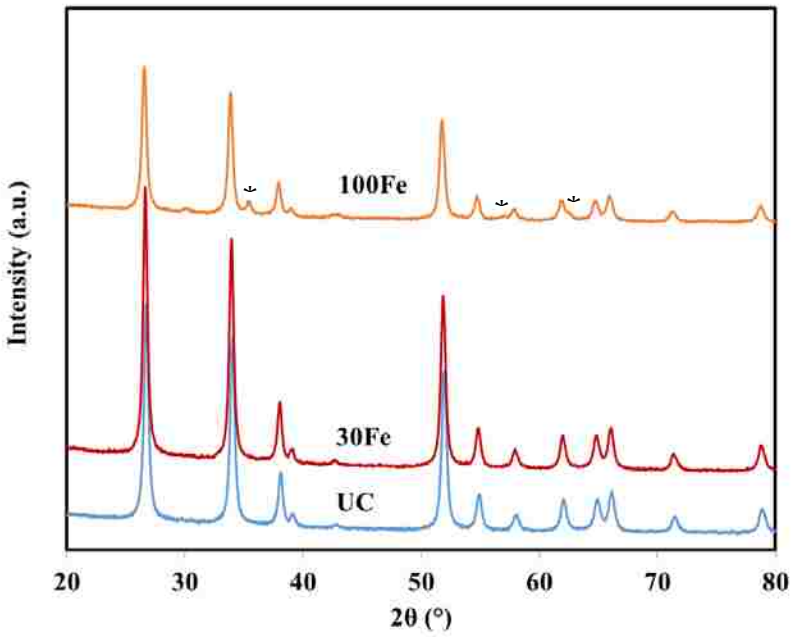

Figure S1. XRD spectra of the uncoated (UC), 30 cycles of iron oxide ALD (30Fe), and 100 cycles of iron oxide ALD (100Fe) coated SnO_2 particles. * represents new peaks with low intensity

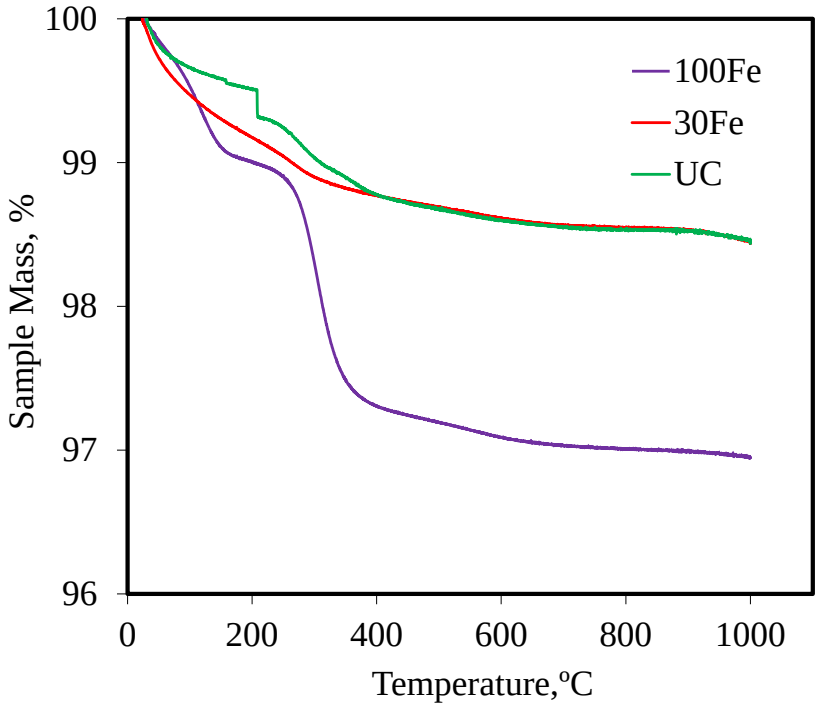

Figure S2. Thermogravimetric analysis (TGA) of the uncoated (UC), 30 cycles of iron oxide ALD (30Fe), and 100 cycles of iron oxide ALD (100Fe) coated SnO_2 particles performed under O_2 with a step increase of 10°C/min

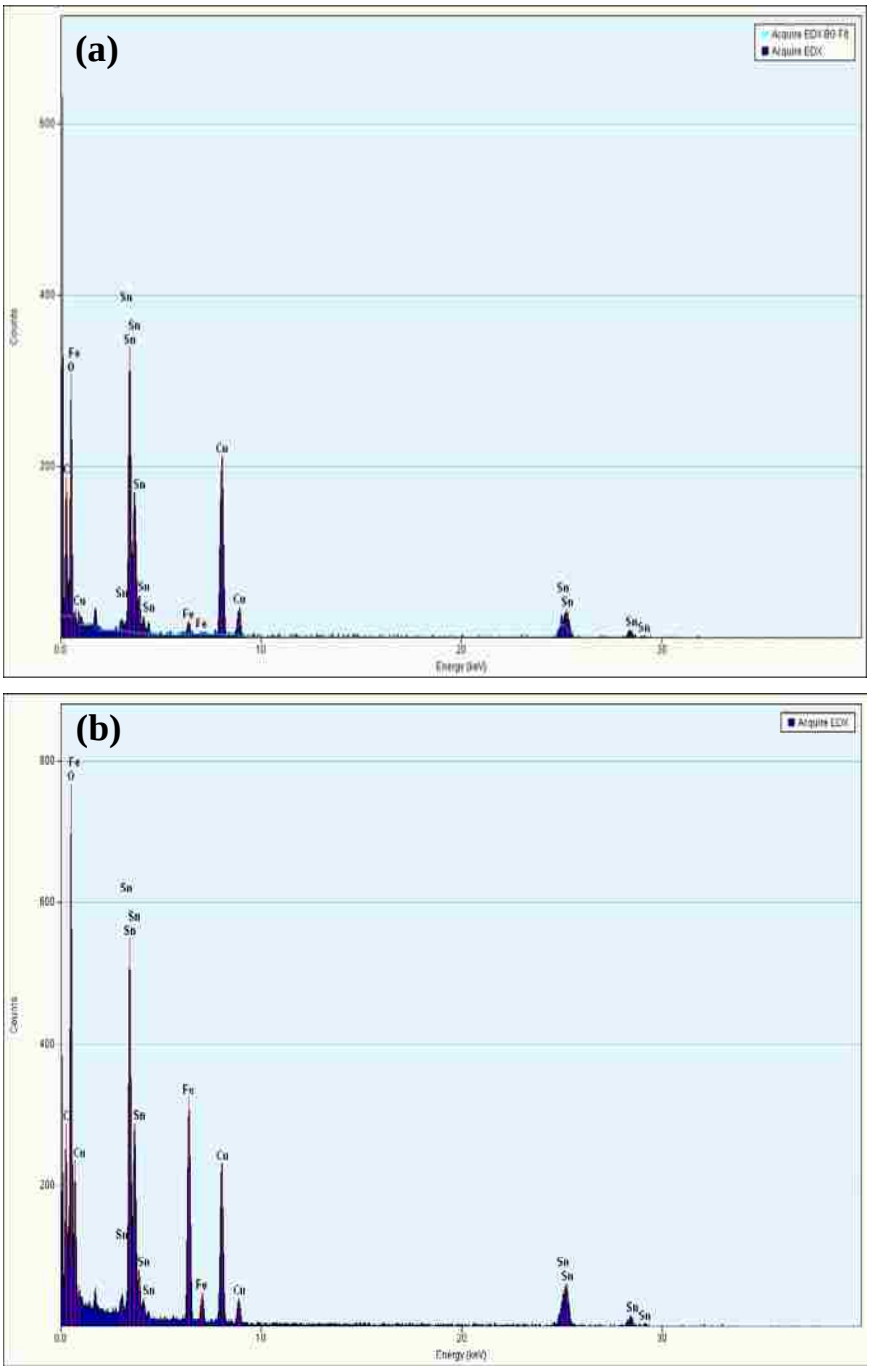

Figure S3. EDS spectra of (a) 30Fe, and (b) 100Fe coated SnO_2 particles

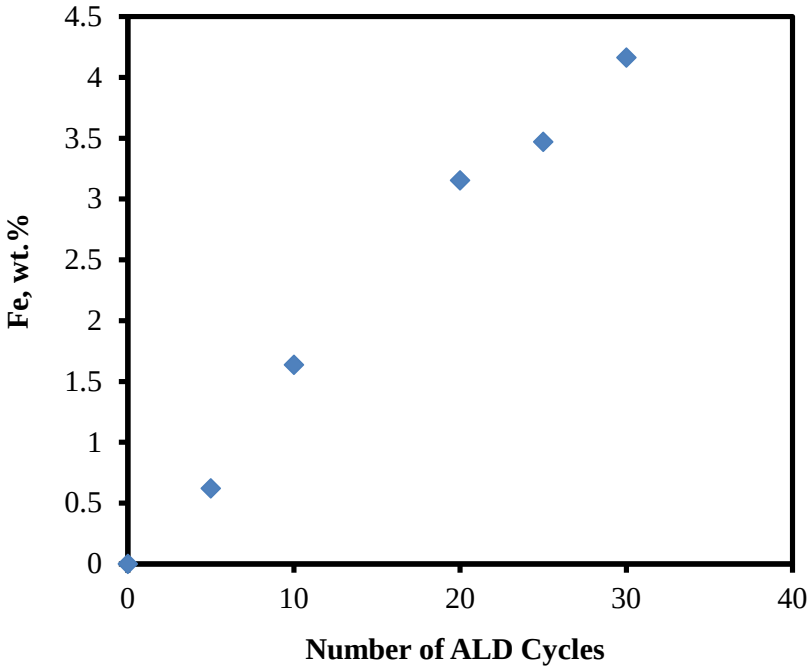

Figure S4. Fe content versus the number of iron oxide ALD coating cycles, as obtained from ICP-AES analysis

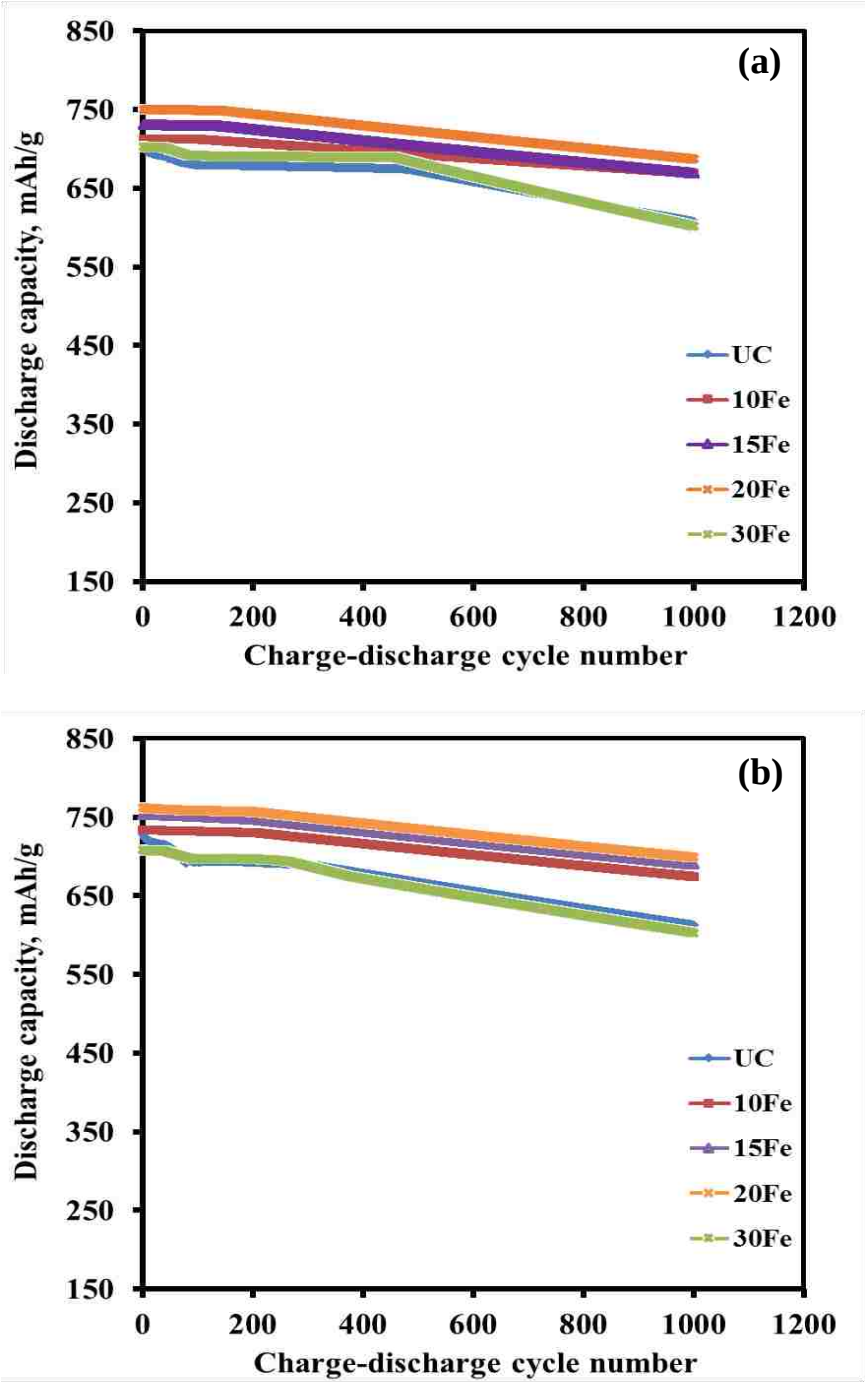

Figure S5. Galvanostatic discharge capacities of SnO_2 particles coated with various thicknesses of iron oxide ALD films at a current density of 250 mA/g between 0.5-3 V at (a) room temperature and (b) 55 $^{\circ}$C

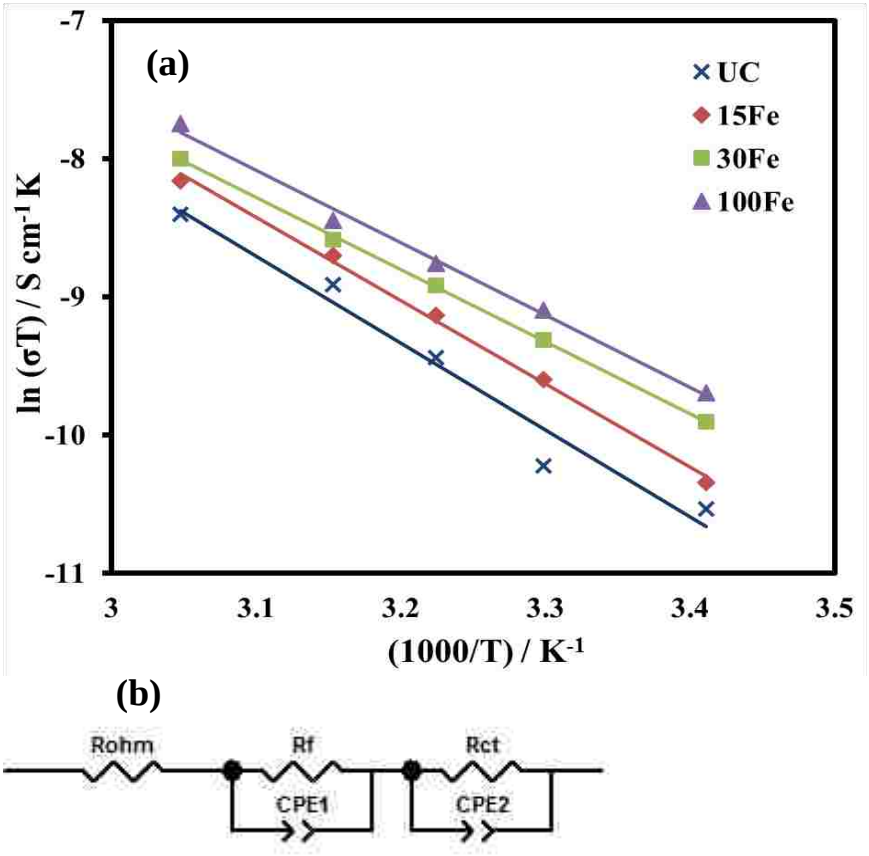

Figure S6. (a) Arrhenius plot of uncoated and 15Fe, 30Fe, 100Fe coated SnO_2 particles for the effects of temperature on conductivity, (b) equivalent circuit for impedance spectra

Iron oxide film phase characterization

XRD analysis was performed on the 30Fe and 100Fe samples to determine the phase of iron oxide ALD films deposited on tin oxide particles. The XRD spectra of the 30Fe and 100Fe samples were compared to that of the uncoated (UC) sample (Figure S1). In both spectra, the diffraction peaks at 26.5, 33.8, 38.2, 51.8, 54.8, 58.2, 61.7, 64.8, 66.1, 71.8 and 78.8^o depict the (110), (101), (200), (211), (220), (002), (310), (112), (301), (202) and (321) crystal planes of the rutile phase SnO_2 (JCPDS No. 41-1445). The XRD analysis showed that there was no significant difference between the spectra of the UC

and 30Fe samples. The observation of similarity in XRD spectra of iron oxide coated and uncoated SnO_2 particles was also reported by El-Shiwani et al.[1] However, the XRD analysis of the 100Fe sample showed evidence of low intensity new peaks (denoted by * in Figure S1) at 30.9 and 61.8º, corresponding to (220) and (440) crystal planes of Fe_3O_4 (JCPDS No. 75-0033). These peaks also match with (220) and (440) planes of α-Fe_2O_3 (JCPDS No. 80-2377). Hence, in this study, the phase of the iron oxide in the ultrathin film cannot be interpreted without ambiguity. The other low intensity new peak at 37.9º can match with any form or phase of iron oxide. Khalr and coworkers[2] also observed that XRD spectra of thin iron oxide coating on fluorine doped tin oxide (FTO) by ALD had weak signals for iron oxide and hence, the phase could not be interpreted without ambiguity.

Thermogravimetric analysis (TGA) under O_2 with a step increase of 10°C/min was performed on the 30Fe and 100Fe sample to interpret the phase of iron oxide (Figure S2). The TGA curve of the UC sample was used as a baseline to compare the 30Fe and the 100Fe samples. For all the samples, the initial weight loss occurred due to removal of physically adsorbed water. The TGA curves of the 30Fe and the UC samples show a total weight loss of ~1.6% at 400°C, which is mainly due to loss of physically adsorbed water (< 200°C) and dehydration of surface hydroxyl groups (> 200°C). Above 400°C, the curve remains stable with no apparent weight loss or gain. In case of the 100Fe sample, the total weight loss was higher at ~3%, most of which had already occurred at 400°C. Above this temperature, the curves show no apparent weight loss or gain. If there was mass gain, the phase of iron oxide would be FeO or Fe_3O_4 as there would be mass gain from its oxidation. The oxidation of FeO to Fe_3O_4 or Fe_3O_4 to Fe_2O_3 normally occurs

above 120°C and 200°C in presence of oxygen respectively. However, there was no mass gain observed in the TGA curves of both the 30Fe and the 100 Fe samples. Theoretically, by using the content of Fe from the ICP-AES data and assuming the film to be entirely Fe_3O_4, the expected mass gain in case of the 30Fe and the 100 Fe samples is 0.19 % and 0.38 % respectively. Assuming the film to be entirely FeO, the mass gain in case of the 30Fe and the 100 Fe samples is 0.59 % and 1.14 %, respectively. This expected mass gain is less than the mass loss of water removal and hence cannot be seen in the TGA curves. The higher mass loss in case of the 100Fe sample was due to presence of more surface hydroxyl groups because of thicker iron oxide film. Herein, since the phase of iron oxide could not be confidently identified, which is similar to the XRD results and hence, it is referred as FeO_x in the paper.

Conductivity measurements

Pellets of only UC, 15Fe, 30Fe and 100Fe samples were prepared for mixed ionic and electronic conductivity measurements. The ac complex plane impedance experiment as described in our previous work was conducted on these samples.[3] The impedance planes were obtained using the same impedance analyzer that was used to measure the EIS spectra. Figure S6b depicts the equivalent circuit that was used to fit the impedance spectra. Out of all the samples, the 100Fe sample showed the highest mixed conductivity (Figure S6a). The conductivity plot is found to be linear and to obey the Arrhenius equation,

$$\sigma \cdot T = \sigma_0 \cdot \exp\left(\frac{-E_a}{k_B T}\right)$$

where, σ_0 is the pre-exponential factor, k_B is the Boltzmann contant, T is the absolute temperature, and E_a is the activation energy for Li ion movement. Figure S6a shows the direct corelation between the mixed conductivity and the temperature (a linear Arrhenius plot). Since the testing temperature were limited to 328 K, there was no phase or structural change observed during the measurements.

References

1. H. El-Shinawi, A. S. Schulze, M. Neumeier, T. Leichtweiß and J. Janek, *The Journal of Physical Chemistry C*, 2014, 118, 8818-8823.

2. B. M. Klahr, A. B. F. Martinson and T. W. Hamann, *Langmuir*, 2011, 27, 461-468.

3. R. L. Patel, H. Xie, J. Park, H. Y. Asl, A. Choudhury and X. Liang, *Advanced Materials Interfaces*, 2015, 2, 1500046

SECTION

2. CONCLUSION AND FUTURE WORK

The optimally thick iron oxide coated sample showed excellent performance at high current densities for long charge-discharge cycles in a practical voltage window. The enhancement of kinetics for Li^+ at the interface due to the conductive film coated by ALD process is novel and can be applied to other Li-ion battery cathode and anode materials.

Even though much of alloying reaction for tin oxide occurs well below tested practical voltage window, tin oxide delivered near theoretical capacity. It is proposed that the irreversible conversion reaction was partially or completely reversible that contributed to the delivered capacity. The mechanism has to be investigated for a better understanding of tin oxide's electrochemical performance in the practical voltage window. Also, the effect of different voltage windows on tin oxide's electrochemical performance needs to be studied.

REFERENCES

1. Megahed, S.; Scrosati, B., Lithium-ion rechargeable batteries. *Journal of Power Sources* **1994,** 51, (1-2), 79-104.

2. Idota, Y.; Kubota, T.; Matsufuji, A.; Maekawa, Y.; Miyasaka, T., Tin-based amorphous oxide: a high-capacity lithium-ion-storage material. *Science* **1997,** 276, (5317), 1395-1397.

3. Courtney, I. A.; Dahn, J., Key Factors Controlling the Reversibility of the Reaction of Lithium with SnO_2 and Sn_2BPO_6 Glass. *Journal of The Electrochemical Society* **1997,** 144, (9), 2943-2948.

4. Brousse, T.; Retoux, R.; Herterich, U.; Schleich, D., Thin-Film Crystalline SnO_2-Lithium Electrodes. *Journal of The Electrochemical Society* **1998,** 145, (1), 1-4.

5. Suntola, T., Atomic layer epitaxy. *Thin Solid Films* **1992,** 216, (1), 84-89.

6. Ma, L.; Nuwayhid, R. B.; Wu, T.; Lei, Y.; Amine, K.; Lu, J., Atomic Layer Deposition for Lithium-Based Batteries. *Advanced Materials Interfaces* **2016**.

7. Scott, I. D.; Jung, Y. S.; Cavanagh, A. S.; Yan, Y.; Dillon, A. C.; George, S. M.; Lee, S.-H., Ultrathin coatings on nano-$LiCoO_2$ for Li-ion vehicular applications. *Nano letters* **2010,** 11, (2), 414-418.

8. Jung, Y. S.; Cavanagh, A. S.; Dillon, A. C.; Groner, M. D.; George, S. M.; Lee, S.-H., Enhanced stability of $LiCoO_2$ cathodes in lithium-ion batteries using surface modification by atomic layer deposition. *Journal of The Electrochemical Society* **2010,** 157, (1), A75-A81.

9. Cheng, H.-M.; Wang, F.-M.; Chu, J. P.; Santhanam, R.; Rick, J.; Lo, S.-C., Enhanced cycleabity in lithium ion batteries: Resulting from atomic layer depostion of Al_2O_3 or TiO_2 on $LiCoO_2$ electrodes. *The Journal of Physical Chemistry C* **2012,** 116, (14), 7629-7637.

10. Guan, D.; Jeevarajan, J. A.; Wang, Y., Enhanced cycleability of LiMn2O4 cathodes by atomic layer deposition of nanosized-thin Al2O3 coatings. *Nanoscale* **2011,** 3, (4), 1465-1469.

11. Zhao, J.; Wang, Y., Ultrathin surface coatings for improved electrochemical performance of lithium ion battery electrodes at elevated temperature. *The Journal of Physical Chemistry C* **2012,** 116, (22), 11867-11876.

12. Patel, R. L.; Xie, H.; Park, J.; Asl, H. Y.; Choudhury, A.; Liang, X., Significant Capacity and Cycle-Life Improvement of Lithium-Ion Batteries through Ultrathin Conductive Film Stabilized Cathode Particles. *Advanced Materials Interfaces* **2015,** 2, (8).

13. Kraytsberg, A.; Drezner, H.; Auinat, M.; Shapira, A.; Solomatin, N.; Axmann, P.; Wohlfahrt-Mehrens, M.; Ein-Eli, Y., Atomic Layer Deposition of a Particularized Protective MgF2 Film on a Li-Ion Battery $LiMn_{1.5}Ni_{0.5}O_4$ Cathode Powder Material. *ChemNanoMat* **2015,** 1, (8), 577-585.

14. Fang, X.; Ge, M.; Rong, J.; Che, Y.; Aroonyadet, N.; Wang, X.; Liu, Y.; Zhang, A.; Zhou, C., Ultrathin surface modification by atomic layer deposition on high voltage $LiMn_{1.5}Ni_{0.5}O_4$ cathode for lithium ion batteries. *Energy Technology* **2014,** 2, (2), 159-165.

15. Kim, J. W.; Kim, D. H.; Oh, D. Y.; Lee, H.; Kim, J. H.; Lee, J. H.; Jung, Y. S., Surface chemistry of $LiMn_{1.5}Ni_{0.5}O_4$ particles coated by Al_2O_3 using atomic layer deposition for lithium-ion batteries. *Journal of Power Sources* **2015,** 274, 1254-1262.

16. Patel, R.; Park, J.; Liang, X., Ionic and Electronic Conductivities of Atomic Layer Deposition Thin Film Coated Lithium Ion Battery Cathode Particles. *RSC Advances* **2016**.

17. Mohanty, D.; Dahlberg, K.; King, D. M.; David, L. A.; Sefat, A. S.; Wood, D. L.; Daniel, C.; Dhar, S.; Mahajan, V.; Lee, M., Modification of Ni-Rich FCG NMC and NCA Cathodes by Atomic Layer Deposition: Preventing Surface Phase Transitions for High-Voltage Lithium-Ion Batteries. *Scientific reports* **2016,** 6.

18. Snyder, M. Q.; Trebukhova, S. A.; Ravdel, B.; Wheeler, M. C.; DiCarlo, J.; Tripp, C. P.; DeSisto, W. J., Synthesis and characterization of atomic layer deposited titanium nitride thin films on lithium titanate spinel powder as a lithium-ion battery anode. *Journal of power sources* **2007,** 165, (1), 379-385.

19. Kohandehghan, A.; Kalisvaart, P.; Cui, K.; Kupsta, M.; Memarzadeh, E.; Mitlin, D., Silicon nanowire lithium-ion battery anodes with ALD deposited TiN coatings demonstrate a major improvement in cycling performance. *Journal of Materials Chemistry A* **2013,** 1, (41), 12850-12861.

20. Lotfabad, E. M.; Kalisvaart, P.; Kohandehghan, A.; Cui, K.; Kupsta, M.; Farbod, B.; Mitlin, D., Si nanotubes ALD coated with TiO_2, TiN or Al_2O_3 as high performance lithium ion battery anodes. *Journal of Materials Chemistry A* **2014,** 2, (8), 2504-2516.

21. Guan, C.; Wang, X.; Zhang, Q.; Fan, Z.; Zhang, H.; Fan, H. J., Highly stable and reversible lithium storage in SnO_2 nanowires surface coated with a uniform hollow shell by atomic layer deposition. *Nano letters* **2014,** 14, (8), 4852-4858.

22. Yesibolati, N.; Shahid, M.; Chen, W.; Hedhili, M. N.; Reuter, M. C.; Ross, F. M.; Alshareef, H. N., SnO_2 Anode Surface Passivation by Atomic Layer Deposited HfO_2 Improves Li-Ion Battery Performance. *Small* **2014,** 10, (14), 2849-2858.

VITA

Sai Abhishek Palaparty was born in Maharashtra, India. In May 2014, he received his Bachelor's degree in Chemical Engineering from National Institute of Technology Warangal, India. He then joined Missouri University of Science and Technology (formerly the University of Missouri – Rolla) in Spring 2015. During Summer 2016, he was an intern at Pennsylvania State University where he worked on Li-ion battery systems. He completed his Master of Science degree in Chemical Engineering from Missouri S&T in December 2016.